

Convex Approximation of Probabilistic Reachable Sets from Small Samples Using Self-supervised Neural Networks

Jun Xiang, Jun Chen, *Senior Member, IEEE*

Abstract—Probabilistic Reachable Set (PRS) plays a crucial role in many fields of autonomous systems, yet efficiently generating PRS remains a significant challenge. This paper presents a learning approach to generating 2-dimensional PRS for states in a dynamic system. Traditional methods such as Hamilton-Jacobi reachability analysis, Monte Carlo, and Gaussian process classification face significant computational challenges or require detailed dynamics information, limiting their applicability in realistic situations. Existing data-driven methods may lack accuracy. To overcome these limitations, we propose leveraging neural networks, commonly used in imitation learning and computer vision, to imitate expert methods to generate PRS approximations. We trained the neural networks using a multi-label, self-supervised learning approach. We selected the fine-tuned convex approximation method as the expert to create expert PRS. Additionally, we continued sampling from the distribution to obtain a diverse array of sample sets. Given a small sample set, the trained neural networks can replicate the PRS approximation generated by the expert method, while the generation speed is much faster.

Note to Practitioners—Reachability analysis is one of the popular methods for solving real-time motion planning problems for dynamic systems under uncertainty while ensuring safety. However, determining the reachable set is challenging. Traditional methods are computationally expensive and often require extensive system information. Meanwhile, neural networks have been shown to construct distributions effectively. Hence, we propose leveraging the capability of neural networks to model the distribution of reachable sets. To simplify the creation of training datasets, we incorporate self-supervised learning in training the neural network. The proposed method offers several advantages: it is easy to use, generates accurate results quickly, and requires less system information. However, as neural networks are statistical methods relying on data-driven insights, their effectiveness inherently depends on the availability of sufficient historical data for the system.

Index Terms—Probabilistic reachable set, Convex approximation, Deep Learning

I. INTRODUCTION

Autonomous system operations face various uncertainties and hazards [1]. The reachable set approach is an important method in collision avoidance [2], [3], safety verification [4] and path planning [5] for Autonomous systems. However, finding the deterministic reachable sets with 100% confidence level is difficult [6]. Meanwhile, the deterministic reachable sets may be too large and over-conservative to be applicable [7]. Finding the Probabilistic Reachable Set (PRS) is more

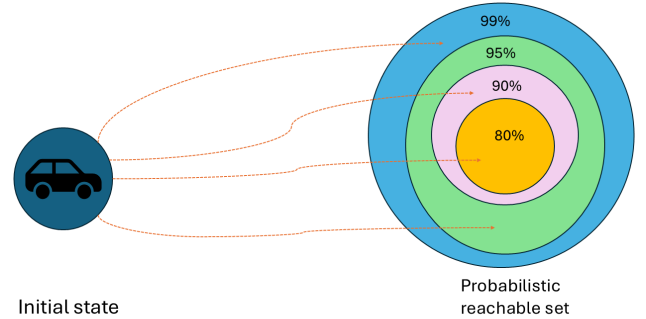


Fig. 1: Probabilistic Reachable set represents the set of possible states a dynamical system can reach from an initial state. For instance, a PRS with a 95% confidence level means that 95% of the possible system trajectories, considering uncertainties or noise, will remain within the set bounds

realistic, incorporating uncertainties and stochastic elements in the system dynamics or initial conditions [8]. A brief visualization of PRS is shown in Fig. 1, where PRS with different confidence levels are colored.

A. Review

Finding PRS remains challenging. One method for determining reachable sets under bounded uncertainties is the Hamilton-Jacobi (HJ) reachability analysis. This approach formulates the problem as a partial differential equation that can be addressed using numerical techniques. Although this method is manageable in scenarios with fewer dimensions, its efficiency significantly diminishes as the dimensionality increases [9] [10]. Additionally, HJ reachability analysis requires detailed information about the dynamics or uncertainties. Meanwhile, strong assumptions are required, such as the absence of time correlations in parameter uncertainties. These limitations make it unsuitable for certain realistic situations [9].

Fortunately, we can identify the reachable sets using a learning-based method given a large dataset from an unknown distribution. Generating a reachable set with machine learning/data-driven has been explored. A trained locally-weighted regression algorithm and nonlinear SVM classifiers can predict the reachability of the two-point boundary value problem (2PBVP) [11]. Other data-driven methods such as the Gauss process [12], Monte Carlo [13], and stochastic

The authors are with the Department of Aerospace Engineering, San Diego State University, San Diego, CA 92182 USA. (emails: jxiang9143@sdsu.edu; jun.chen@sdsu.edu).

disturbance [14] have also been developed to approximate reachable set. However, all of those methods have significant limitations in practice for three aspects: a) they all require a lot of samples to perform; b) they cannot provide fast and accurate probabilistic reachable set with adjustable confidence levels; c) their PRS bound is not convex and linear.

Deep learning technology has seen significant advancements recently in computer vision [15] and nature language process [16]. And those methods are further adopted in many different fields such as finance [17], cyber security [18], healthcare [19], [20] and robotics [21]–[24]. Deep learning-based methods have been effectively applied to solve obstacle avoidance [25] and path planning problems [26], [27], demonstrating their suitability for addressing challenges in autonomous control tasks. The Universal Approximation Theorem [28], guarantees that a feedforward neural network can approximate any nonlinear real-valued function. The advantages of neural networks include their ability to generate complex outputs from simple inputs, as seen in generative models. Previous research shows that neural networks can work when massive data is massively missing [29] and can determine uncertainty [30]. Neural networks can rapidly extract the texture information of pavement from just a few images [31]. Neural networks indeed offer significant advantages in terms of reduced computing time. Also, the parallel nature of neural networks can lead to significant reductions in computing time [32]. Furthermore, Transformers [16] and self-supervised learning have revolutionized the field of artificial intelligence [33] and have become essential tools for developing more efficient, and versatile AI models when limited sample is available [34]. Therefore, we propose designing a transformer-based neural network to generate PRS, and we further employ self-supervised learning techniques to train this network.

B. Contribution

In this paper, we propose a method that uses self-supervised and multi-label training to train a transformer-based neural network for generating convex approximations of PRS from a small number of samples. The numerical experiments prove that the neural network can generate reliable convex approximations when the given samples come from a distribution that has been learned by the network. This effective method relies on just one assumption:

- Assumption 1: a large number of previous samples have been observed before the predicting task.

This assumption is satisfied in many fields such as autonomous driving [35], flight landing prediction [36], and robotics [37]. Our method offers three unique advantages that set it apart from other methods:

- *Advantage 1:* No information about the desired system is needed; only a few samples of the desired distribution are required for PRS generating.
- *Advantage 2:* The generation speed is extremely fast, making it suitable for online applications.
- *Advantage 3:* All the PRS bound generated are convex and linear.

- *Advantage 4:* Very few labeled data are needed for training, which simplifies the training process and makes large-scale training feasible.

II. PROBLEM MODELING

The main goal of the paper is to generate a convex approximation that can capture the PRS of an unknown static uncertainty whose data samples are gradually observed.

In this section, we will introduce and discuss the concepts of reachable sets and PRS associated with a dynamic system with uncertain discrete-time characteristics [38], [39].

Let us consider a general discrete-time dynamic system expressed as

$$\mathbf{s}_{k+1} = \mathbf{f}(\mathbf{s}_k, \mathbf{u}_k, \boldsymbol{\theta}_k, \mathbf{w}_k), \quad (1)$$

where, $\mathbf{s}_k \in \mathbb{R}^2$ denotes the state of the system (we only consider 2d dynamic systems in this paper, we use s instead of x like many other dynamic system research to distinguish x -dimension) at time step $k \in \{1, \dots, T\}$, $\mathbf{u}_k \in \mathcal{U}_k$ denotes an uncertain control input, $\boldsymbol{\theta}_k \in \Theta$ denotes an uncertain parameter, $\mathbf{w}_k \in \mathbb{W}$ denotes an uncertain disturbance, and $\mathbf{s}_0 \in \mathcal{S}_0$ denotes the initial state. Diverging from most previous studies [9], this paper allows the sets $\mathcal{U}_k \subset \mathbb{R}^m$, $\Theta \subset \mathbb{R}^p$, $\mathbb{W} \subset \mathbb{R}^q$, and $\mathcal{S}_0 \subset \mathbb{R}^2$ to be unbounded. Taking into account the uncertainties in \mathbf{s}_k , \mathbf{u}_k , $\boldsymbol{\theta}_k$, and \mathbf{w}_k , it follows that \mathbf{x}_{k+1} becomes a random vector following an unknown probability distribution. Then at time T , the reachable set \mathcal{S}_T of the dynamic system in Eq. 1 is defined to be

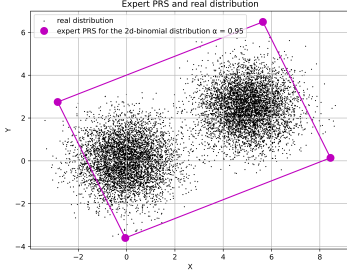
$$\begin{aligned} \mathcal{S}_T := \{ & \mathbf{s}_T \in \mathbb{R}^2 : \mathbf{s}_k = \mathbf{f}(\mathbf{s}_{k-1}, \mathbf{u}_{k-1}, \boldsymbol{\theta}_{k-1}, \mathbf{w}_{k-1}), \\ & \mathbf{s}_0 \in \mathcal{S}_0, \mathbf{u}_{k-1} \in \mathcal{U}_{k-1}, \boldsymbol{\theta}_{k-1} \in \Theta, \mathbf{w}_{k-1} \in \mathbb{W}, \\ & k \in \{1, \dots, T\}, \end{aligned} \quad (2)$$

where \mathbf{s}_0 denotes the initial state and \mathcal{S}_0 denotes the initial set. Observe that because the sets \mathcal{U}_{k-1} , Θ , \mathbb{W} , and \mathcal{S}_0 can be unbounded, the resulting reachable set \mathcal{S}_T could also be unbounded. This implies that determining a bounded set where the state is definitively contained might not be feasible. Therefore, our goal is to generate a bounded set where the probability of the state being within this set exceeds a certain confidence level, which is called a Probabilistic Reachable Set (PRS). At time k , a bounded set $\tilde{\mathcal{S}}_k$ can be qualified as a PRS of the dynamic system defined in Eq. 1 at confidence level α if and only if

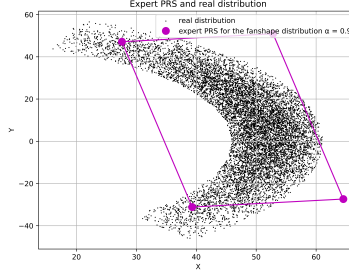
$$\Pr(\mathbf{s}_k \in \tilde{\mathcal{S}}_k) \geq \alpha. \quad (3)$$

It indicates that the probability of the system reaching the PRS at time k exceeds α . For example, if $\alpha = 95\%$ and the system runs an infinite number of times, the system will be outside the PRS less than 5% of the time. When $\alpha = 100\%$ and a PRS $\tilde{\mathcal{S}}_k$ does exist, then the reachable set \mathcal{S}_k defined in Eq. 2 belongs to the $\tilde{\mathcal{S}}_k$.

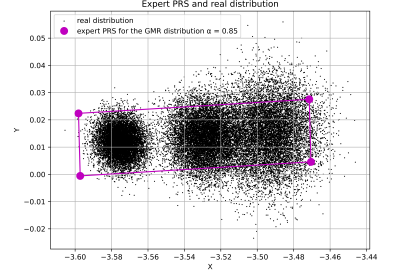
The previous expert method [40] can find multiple $\tilde{\mathcal{S}}_k$ and all the founded $\tilde{\mathcal{S}}_k$ are convex and as tight as possible. We define the set $\tilde{\mathcal{S}}_k$ using the positions of the four vertices, represented as $\tilde{\mathcal{V}}_k \in \mathbb{R}^{4 \times 2}$. The trained neural network should



(a) Example of 2d-binomial distribution and sample expert convex PRS



(b) Example of fan-shape distribution and sample expert convex PRS



(c) Example of GMR trajectory predictor distribution and sample expert convex PRS

Fig. 2: Distribution and convex PRS demo

be able to imitate the expert and generate a similar PRS that has a confidence level close to α , as shown in Eq. 4,

$$\tilde{\mathcal{V}}_k = NN(w, \mathbf{s}_k) \quad (4)$$

where w is the trained weights of the neural network, $\mathbf{s}_k = \{s_k^i\}_{i=1}^n$ is a collection of samples from the real distribution of the reachable set with $s_k^i \sim \mathbf{s}_k$, and n as the number of the samples. The desired n should be smaller than 100.

In the rest of the paper, we only consider the reachable set for a specific single time step, for example, $k = T$. So to simplify the notation, we use \mathcal{S} to refer the actual reachable set, $\tilde{\mathcal{S}}$ to refer the PRS, $\tilde{\mathcal{V}}$ as the four vertices of the PRS, and \mathbf{s} as the state of the system, \mathbf{s} as the collection of samples from the reachable set at desired time point.

III. DATASET AND EXPERT METHOD

A. Target distribution

In this paper, we evaluate the proposed method to determine if it can approximate three different probabilistic distributions, all of which are based on the Gaussian distribution, commonly used in aircraft trajectory modeling [41]. Any sample from the target probabilistic distributions is 2-dimensional data, $\mathbf{s} \in \mathbb{R}^2$.

1) *2d-binomial distribution*: 2d-binomial distribution [38] forms clusters around two different coordinate points. The sampling plot of the 2d-binomial distribution is shown in Fig.2a. The sample process includes two steps, first is randomly selecting one of two center points, second is adding Gaussian noise to both the x- and y-coordinates of the chosen center point. Let $\mathbf{C}_1 = (x_1, y_1)$ and $\mathbf{C}_2 = (x_2, y_2)$ represent the two center points. Let $\mathbf{N} = \begin{pmatrix} N_x \\ N_y \end{pmatrix}$ be the Gaussian noise added to both coordinates, where $N_x \sim \mathcal{N}(0, \sigma^2)$ and $N_y \sim \mathcal{N}(0, \sigma^2)$ are independent Gaussian random variables with mean 0 and variance σ^2 . The sample of the 2d-binomial distribution will be $\mathbf{s} = \mathbf{C}_i + \mathbf{N}$, $i \in \{1, 2\}$. The probability density function(PDF) of the 2d-binomial distribution is easy to calculate:

$$P(\mathbf{s}) = \frac{1}{2} \cdot \mathcal{N}(\mathbf{s}|\mathbf{C}_1, \sigma^2\mathbf{I}) + \frac{1}{2} \cdot \mathcal{N}(\mathbf{s}|\mathbf{C}_2, \sigma^2\mathbf{I}), \quad (5)$$

where, $\mathcal{N}(\mathbf{s}|\mathbf{C}_i, \sigma^2\mathbf{I})$ represents the bivariate Gaussian distribution centered at $\mathbf{C}_i = (x_i, y_i)$ with covariance matrix $\sigma^2\mathbf{I}$ (identity matrix scaled by σ^2 , meaning independent noise with the same variance for x and y).

2) *Fanshape distribution*: The fan-shape distribution [38] represents points sampled from a distribution of motion paths influenced by truncated normal distributions of speed and direction, capturing realistic variations in both parameters. The sampling plot of the fanshape distribution is shown in Fig.2b.

Fanshape distribution is based on the Dubins vehicle model of flight. The speed of the flight follows a truncated Gaussian distribution $v \sim \mathcal{N}(\mu_1, \sigma_1)$ with $\mu_1 = 190$ km/h and $\sigma_1 = 5$ km/h, and the value of speed constrained to the interval [165, 220] km/h. Similarly, The heading angle of the vehicle is sampled from another truncated Gaussian distribution $\theta \sim \mathcal{N}(\mu_2, \sigma_2)$ with $\mu_2 = 10^\circ$ and $\sigma_2 = 30^\circ$, and the range of heading angle is $[-50^\circ, 70^\circ]$.

The position $\mathbf{s} := [x_k, y_k]^\top$ of the flight at time k is modeled by the following discrete-time dynamic system:

$$\begin{bmatrix} x_k \\ y_k \end{bmatrix} = \begin{bmatrix} x_{k-1} \\ y_{k-1} \end{bmatrix} + \begin{bmatrix} \cos \theta \\ \sin \theta \end{bmatrix} v \Delta t,$$

where $[x_{k-1}, y_{k-1}]^\top$ is the position of the flight at the previous time step $k-1$. $[x_k, y_k]^\top$ is the position of the flight at the time step k . v is the speed and θ is heading angle. Due to the uncertainties in v and θ , the position \mathbf{s} is a random vector that obeys a non-Gaussian distribution, which is referred to as the fanshaped distribution. The PDF of the position is difficult to derive.

3) *GMR trajectory predictor*: GMR trajectory predictor can regress the possibility distribution of the future position of flight near terminal [42] with multiple Gaussian distributions given the past trajectory. The sampling plot of the GMR trajectory predictor distribution is shown in Fig.2c. The regressed conditional possibility distribution of the future position of flight is defined by the following equation:

$$P(\mathbf{s} | \mathbf{s}^{past}) = \sum_{k=1}^K \pi_{\mathbf{s} | \mathbf{s}_k^{past}} \mathcal{N}_k(\mathbf{s} | \boldsymbol{\mu}_{\mathbf{s} | \mathbf{s}_k^{past}}, \boldsymbol{\Sigma}_{\mathbf{s} | \mathbf{s}_k^{past}}), \quad (6)$$

where where $\mathcal{N}_k(s | \mu_{s|s_k^{past}}, \Sigma_{s|s_k^{past}})$ are Gaussian distributions with mean $\mu_{s|s_k^{past}}$ and covariance $\Sigma_{s|s_k^{past}}$, K is the number of Gaussians, and, s_k^{past} is the input and s is the output, where s_k^{past} is the combined past trajectory and future trajectory guide of the ego agent. s is the trajectory prediction. $\pi_k \in [0, 1]$ are weights that sum up to one. If π_k is larger, the more likely the s belongs to \mathcal{N}_k . We use three-time step prediction as the desired distribution.

B. Expert method

The expert method is proposed in [40]. The expert method can generate the PRS of an uncertain dynamic system. This data-driven method builds on a kernel density estimator (KDE) that can generate the PRS, accelerated by a fast Fourier transform (FFT). These KDE values are then utilized within an Integer Linear Programming (ILP) framework to find a minimal parallelogram box that approximates the probabilistic geofence. This ILP solution effectively encapsulates the area where the state is expected to stay with high confidence.

A brief process of the ILP Heuristic Algorithm is shown in the Algorithm 1.

Algorithm 1 ILP Heuristic Algorithm

```

1: function BOXAPPROX( $r_{\min}, c_{\min}, r_{\max}, c_{\max}, \omega_{ij}$ )
2:    $\omega'_{ij} \leftarrow \omega_{ij}, \text{copy}()$ 
3:    $z_{ij}[1 : N][1 : N] \leftarrow 0$ 
4:    $r_{\min}, c_{\min} \leftarrow \arg \max_{i,j} \omega'_{ij}$ 
5:    $r_{\max} \leftarrow r_{\min}, c_{\max} \leftarrow c_{\min}$ 
6:   while  $\sum_{i=1}^N \sum_{j=1}^N \omega_{ij} z_{ij} < \alpha \sum_i \sum_j \omega_{ij}$  do
7:      $i, j \leftarrow \arg \max_{i,j} \omega'_{ij}$ 
8:      $\omega'_{ij}[i, j] \leftarrow 0.0$ 
9:      $r_{\min} \leftarrow \min(r_{\min}, i), r_{\max} \leftarrow \max(r_{\max}, i)$ 
10:     $c_{\min} \leftarrow \min(c_{\min}, j), c_{\max} \leftarrow \max(c_{\max}, j)$ 
11:     $z_{ij}[r_{\min} : r_{\max}][c_{\min} : c_{\max}] \leftarrow 1$ 
12:   end while
13:   return  $z_{ij}$ 
14: end function

```

The ILP Heuristic Algorithm approximates solutions for integer linear programming problems using heuristics. It starts with a weight matrix ω_{ij} and a zero matrix z_{ij} , setting initial indices based on ω_{ij} 's maximum values. The algorithm loops to update z_{ij} until the product of z_{ij} and ω_{ij} meets a threshold α . Each iteration zeros out the maximum ω_{ij} and adjusts boundary indices. The corresponding z_{ij} entry is set to one within these boundaries, yielding the matrix as an efficient approximation of the ILP solution. The expert convex generated is shown in Fig. 2. The black points represent the distribution and purple convex covers a desired percent of the distribution.

C. Training dataset generation

Theoretically, there are unlimited correct convex approximations for PRS given a probability distribution. At the same time, the expert method introduced in the previous section can generate a very accurate convex approximation

if enough samples are given. Therefore, for each distribution P and each desired confidence level α , we can generate a set of correct convex approximation $\tilde{\mathbf{S}}_{P,\alpha} = \{\tilde{\mathbf{S}}_{P,\alpha}^i\}_{i=1}^n$. In this paper, the correct convex approximation has 1% error toleration. Therefore, we consider the approximation is correct if $\alpha + 0.01 \geq \Pr(s \in \tilde{\mathbf{S}}_{P,\alpha}) \geq \alpha$. Each correct convex approximation $\tilde{\mathbf{S}}_{P,\alpha}$ is defined by four vertices $\tilde{\mathbf{V}}_{P,\alpha}$. Then the set of vertices of the correct convex approximation is denoted as $\tilde{\mathbf{V}}_{P,\alpha} = \{\tilde{\mathbf{V}}_{P,\alpha}^i\}_{i=1}^n$. The usage of the generated correct convex approximation will be introduced in the method section below.

IV. METHOD

A. Self-supervised learning

Previous research [33] has proven that the transformer can process the visible (unmasked) parts of the data, reconstructing the entire input from the encoded, incomplete data (masked data). Therefore, if we only have a few samples from the distribution, the transformer may be able to reconstruct the entire distribution.

As the previous section III, we have the vertices of expert convex approximation $\tilde{\mathbf{V}}_{P,\alpha}$. Fig.3 shows the examples of how we mask the distribution. During the training, we randomly mask most of the sample points, only leaving a few samples visible to the transformer, and ask the transformer to generate the corresponding PRS.

With this self-supervised learning strategy, we are able to show many sets of visible samples of one distribution to the neural networks. When we show the stranger samples to the trained neural networks, the trained neural network is able to identify the distribution by recognizing and relating the visible samples to the samples the neural networks have seen during the training process.

B. Multi-label learning and loss function

As introduced in section II, one distribution can have multiple correct convex approximations. Therefore, we can use multi-label learning instead of single-label learning. Multi-label learning not only reduces computational overhead but also allows the model to share learned features across multiple labels, potentially leading to better generalization. Fig. 4 shows an example of multi-label learning. The neural network generated an output based on the current weights of the neural network. Then the losses between each expert and the output are calculated and the smallest loss will be used to train the neural network. For the real training, we will have more expert PRS samples. Like many regression machine learning research studies, we use the MSE loss function as shown in Eq. 7. MSE loss can help the neural network minimize the average error between the expert and the output.

$$\text{Loss} = \min_{j \in [1,10]} \frac{1}{8} \sum_{i=1}^8 (\hat{y}_{ij} - y_i)^2 \quad \text{where } \hat{y}_{ij} \in \tilde{\mathbf{V}}_{P,\alpha} \quad (7)$$

where:

- we have 8 (four 2d vertices) elements in the output vector,
- y_i is the generated value for the i -th element,
- \hat{y}_{ij} is the j -th expert vertices for the i -th element.

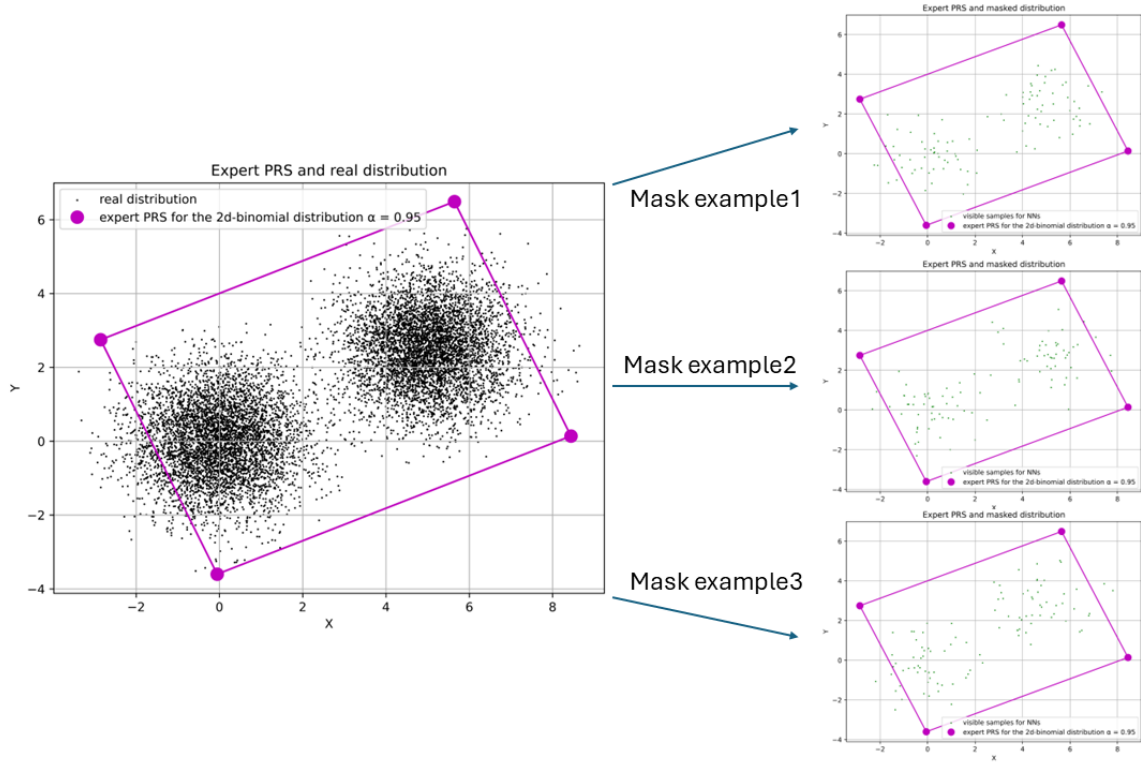


Fig. 3: Masked distribution: we only show a few samples to the neural networks, and ask neural networks to generate the corresponding PRS.

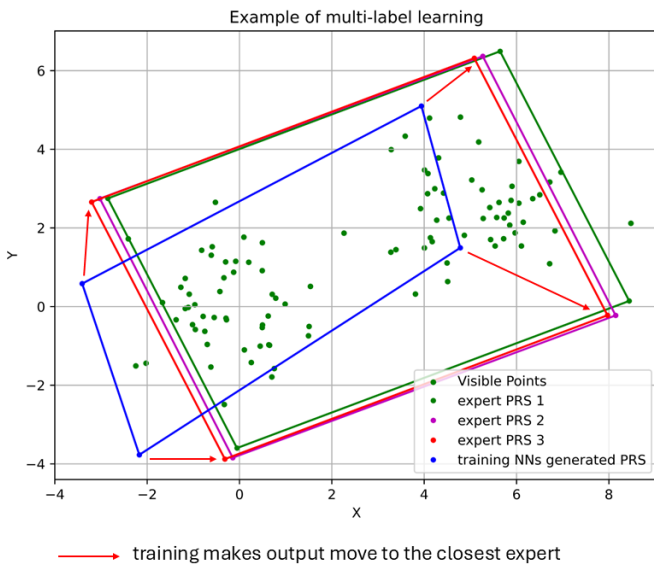


Fig. 4: Example of multi-label learning

C. Neural networks architecture

The overall architecture of the neural network we used is shown in Fig. 5, which is designed based on our previous work [43]. The input to the neural network consists of sampled points and the desired confidence level. Before sending these inputs to the neural network, we normalize them first. The

confidence level and the sample points are then embedded in a higher dimension using a linear layer. The embedded items are concatenated together. These concatenated embeddings are then sent to the transformer layer. In the transformer, the channel representing the confidence level interacts with all the point channels. Finally, we send the confidence level channel to an output layer, resulting in four vertices of the convex hull.

D. Input normalization, embedding, and concatenate

Because sample points are drawn from different distributions, they have very different means and variances, which can cause challenges for the training process of neural networks. Normalizing those points before feeding them into the neural network is very crucial for several reasons. First, if certain inputs have larger values and higher variance than others, they may dominate the training process. For example, if one target (or feature) has a very large value compared to others, its gradient will be disproportionately large. Second, normalization can accelerate the training process. When the scales of the inputs are not consistent, the model might spend more time adjusting weights to accommodate the varying scales of input data rather than learning meaningful patterns. Third, normalization can prevent overfitting by reducing bias toward dominant features and indirect regularization effects.

We use the Min-Max scaling [44] to normalize the sample points. The Min-Max scaling equation is defined by:

$$x' = \frac{x - \min(x)}{\max(x) - \min(x)}. \quad (8)$$

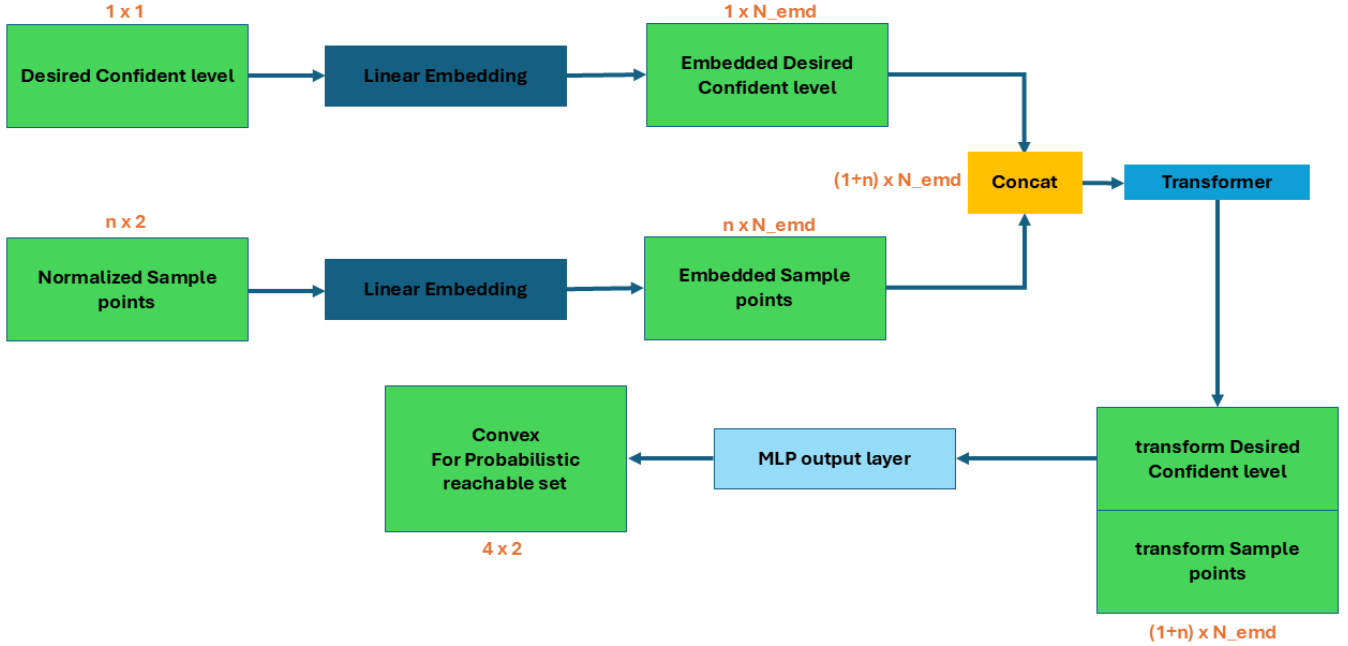


Fig. 5: Neural network architecture

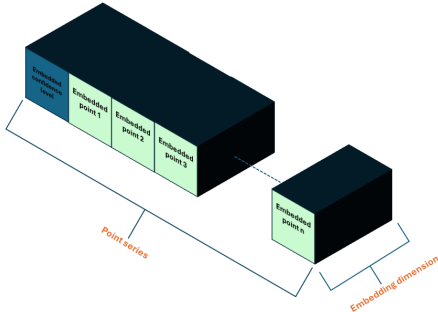


Fig. 6: Concatenated tensor

Min-max scaling scales sample points to the range $[0, 1]$ without changing the relative position between points. At the same time, since all the points are sampled from a reasonable distribution, so no outlier can heavily influence the normalization.

After normalizing, we use a single linear layer to embed the inputs. Compared to vision or natural language inputs, the inputs in our task are much more straightforward to understand. We primarily aim to determine the relationship between points rather than to interpret their meanings. Additionally, the transformer model already incorporates non-linearities. Therefore, we choose to embed the inputs into relatively low dimensions and use only a single linear layer to decrease the computing complexity.

After embedding, the point tensor has dimensions $(N,$

$C)$, where N is the dimension of the series of points and C is commonly referred to as the channel in the field of machine learning. We concatenated the confidence level tensor and the point tensor together along the N dimension. So, the concatenated tensor has dimensions $(N + 1, C)$, while the first channel is the channel of the confidence level. The concatenated tensor then looks like the Fig. 6.

E. Transformer

For this work, we only use the transformer encoder [16] since we output the vertex at once instead of one by one. The encoder is composed of a stack of 6 identical layers, each layer has two sub-layers, a multi-head self-attention mechanism, and the feedforward network. We also kept the residual connection and layer normalization. Compared to other popular layers, such as the recurrent and convolutional layers, self-attention has three main advantages. First, self-attention has lower computational complexity per layer. Second, it requires fewer sequential operations since most computations can be parallelized. The third advantage is that self-attention can learn the dependencies between two points that are far from each other. For example, if we use CNNs, we may input points patch by patch, then it is difficult to learn the relationship between the first patch and the last patch. In contrast, each point interacts with all the other points at the same time in self-attention.

F. Output

In the previous masked autoencoder research. Mask tokens are introduced after the encoder, so the decoder will know

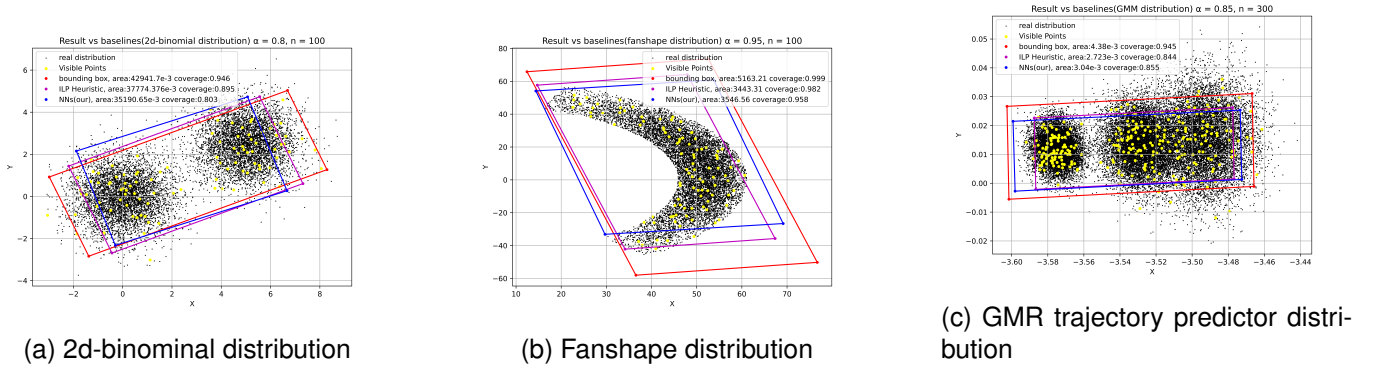


Fig. 7: Example outputs if three methods take the same visible points, visible points are enlarged as yellow points for greater visibility.

which missed position is required to be generated. However, unlike reconstructing assignments, we do not have mask tokens. We do not know the visible samples are from which part. In fact, unlike CV and NLP problems, the sequence does not matter in our problem. For example, "The dog chased the cat" and "The cat chased the dog" are two completely different sentences, even though they have exactly the same words. In contrast, in our problem, the point set $[(1, 1), (2, 2)]$, and $[(2,2), (1, 1)]$ have the same distribution. Therefore, no additional global context is required. Furthermore, the goal of the proposed neural network is to generate a convex bound instead of reconstructing the whole distribution. All in all, a simple output layer is enough to generate the convex bound with the features captured from the visible samples.

We use a multilayered output like ViT [15] instead of a single linear layer like the original transformer. The multi-layer output can further process the features extracted from the points channels and refine the final classification. We only used the transformed confidence level channel to output. The transformer allows the confidence level channel to attend to all other channels (embedded points), gathering contextual information from all the points. Finally, we need to denormalize the output, since the points we want to bound are normalized.

G. Parameters

For the transformer, embedding dimension N_{emd} is 864. We use 6 attention heads, so each head processes 144 embedding dimensions of each channel. The number of attention layer is also 6. Optimization is performed using the Adam optimizer with a dynamic learning rate to ensure gradual convergence. Additionally, a dropout rate of 0.2 is applied to prevent overfitting by randomly omitting certain neurons during training.

V. RESULT

A. Experiment setting

We compare the proposed method with the ILP Heuristic (ILP), which is the expert method, and the bounding box (BB) method [45] [46], a popular approach to finding a convex approximation of the PRS. Both baseline methods are KDE-based. Fig. 7 are examples of point distribution and convex

hulls generated by different methods given the same visible points. All the experiences are run in Intel(R) Core(TM) i9-12900KF and NVIDIA GeForce RTX 3090.

1) *Training dataset*: In each training iteration, we randomly assign ten sets of expert vertices as the target and randomly pick 100 samples (300 for the GMR trajectory predictor) from the desired distribution as the neural network's input. To accelerate the training process, we prepare 100 sets of expert vertices for each desired confidence level and prepare 320,000 sets of samples before training begins. To make the required expert vertices, it will cost experts about 24 hours for all distributions. In addition to expert vertices generating, we also need to generate training input samples before training. The sample generation time varies across different distributions. For the binomial distribution, it takes only about 2 minutes to generate 320,000 sets of samples. For the fanshape distribution, the process takes approximately 40 minutes to produce the same number of sample sets. In the case of the GMR trajectory predictor, it requires around 30 hours to generate 320,000 sets of samples. Generally, we can prepare the training dataset for a known distribution within a few days. It supports that the *Advantage 4* of the proposed method, the training dataset is easy to make. Additionally, the proposed method exhibits *Advantage 3*: all PRS are guaranteed to be convex and linear, as the neural network is specifically designed to generate only the vertices of convex sets.

2) *PRS generating*: We tested the trained neural networks by presenting them with 5,000 random tasks (1000 for each α) in each distribution. Each task contains 100 (300 for GMR) points of the distribution and has never been seen by the neural network. The neural network will generate the corresponding PRS for those points. At the same time, we also generate PRS with BB and ILP given the same points as the baseline. However, since BB and ILP are not learning-based and do not require a training process, comparing them directly may not be entirely fair. To adjust for this, we also compared the results using PRS generated by BB and ILP with 20 times more samples to thoroughly evaluate our proposed method. Besides the baseline method, we also run the MINLP Optimal Algorithm [47] to determine the smallest area of a convex satisfies the coverage requirement.

2d-binomial	NN(our method)	BB(100)	ILP(100)
confidence level	MSE(range)	MSE(range)	MSE(range)
80%	0.42%(79.12% - 82.05%)	11.04%(87.56% - 99.42%)	3.66%(72.00% - 93.54%)
85%	0.35%(84.45% - 86.63%)	10.18%(91.98% - 99.80%)	3.70%(72.17% - 95.76%)
90%	0.24%(89.51% - 91.01%)	8.20%(93.26% - 99.94%)	4.98%(86.16% - 98.78%)
95%	0.62%(94.08% - 96.29%)	4.20%(94.84% - 99.99%)	3.25%(92.45% - 99.73%)
99%	0.87%(97.66% - 99.94%)	1.87%(97.09% - 99.99%)	0.80%(98.97% - 99.99%)

TABLE I: MSE and range on 2d-binomial distribution distribution compare to baseline with a small number of sample

fanshape	NN(our method)	BB(100)	ILP(100)
confidence level	MSE(range)	MSE(range)	MSE(range)
80%	0.32%(78.95% - 80.44%)	11.98%(80.28% - 99.80%)	2.83%(75.04% - 91.87%)
85%	0.25%(84.44% - 86.21%)	9.88%(85.39% - 99.91%)	2.95%(75.24% - 94.01%)
90%	0.23%(89.40% - 90.91%)	7.36%(89.60% - 99.99%)	2.69%(75.63% - 98.43%)
95%	0.49%(95.22% - 96.02%)	4.32%(92.60% - 100%)	2.20%(85.67% - 99.88%)
99%	0.98%(99.96% - 99.99%)	1.33%(98.03% - 100%)	1.12%(97.86% - 100%)

TABLE II: MSE and range on fanshape distribution distribution compare to baseline with a small number of sample

GMR trajectory predictor	NN(our method)	BB(300)	ILP(300)
confidence level	MSE(range)	MSE(range)	MSE(range)
80%	1.79%(79.54% - 84.27%)	11.31%(84.04% - 96.41%)	2.74%(75.00% - 88.70%)
85%	1.76%(82.34% - 88.25%)	9.56%(88.09% - 98.02%)	2.62%(75.31% - 90.94%)
90%	1.13%(88.31% - 91.8%)	7.37%(93.11% - 99.40%)	1.76%(81.48% - 96.56%)
95%	0.85%(94.14% - 97.83%)	4.09%(95.82% - 99.95%)	1.11%(90.61% - 98.80%)
99%	0.58%(99.18% - 99.94%)	0.80%(98.42% - 100%)	0.40%(97.03% - 99.95%)

TABLE III: MSE and range on GMR trajectory predictor distribution compare to baseline with a small number of sample

3) *PRS evaluating*: To evaluate a PRS, we first need to determine the coverage. To represent the real distribution, we sampled 100,000 points from the desired distribution. The resulting coverage was determined by counting the percentage of these sampled points that fell within the generated PRS.

Mean Squared Error(MSE) is the metric we used to evaluate the accuracy with which the PRS approximates the desired confidence level:

$$\text{MSE} = \frac{1}{n} \sum_{i=1}^n (\alpha_i - \hat{\alpha}_i)^2. \quad (9)$$

α is the coverage of the generated PRS and $\hat{\alpha}_i$ is the desired coverage. n is 1000 because we test 1000 times for each α . We also recorded the minimum and maximum coverage values to evaluate performance stability. While a low MSE indicates that the PRS is accurate, it does not guarantee correctness. Therefore, it is essential to compare the percentage of instances where the PRS exceeds the desired coverage. We called it the correctness rate.

4) *Generating time*: Generating time is a crucial property in deciding whether a method can be used in online applications. Therefore, we compare the time to generate one correct PRS by each method.

B. Compare coverage accuracy, correctness, and area to baseline

First, we aim to evaluate whether the proposed method can effectively produce accurate PRS. Table I presents the MSE and range comparisons between the proposed method and two baseline approaches, given the exact same visible points on the 2d binomial distribution. Our method consistently achieves lower MSE and a narrower range than the baseline methods, except at a 99% confidence level, where its performance closely matches that of ILP. Table II shows the MSE and range results on the fanshape distribution.

The proposed method demonstrates exceptional performance, with significantly lower MSE and a tighter range across all confidence levels. Finally, Table III corroborates the findings from the previous tables, further showcasing that the proposed method achieves substantially lower MSE and a consistently tighter range, underscoring its superior performance. All in all, we found out that our method can produce very accurate PRS. All MSE is lower than 1%, with smaller intervals, indicating our method is very stable and consistent. In contrast, KDE-based baseline methods have higher MSE and variance especially when the desired confidence level is lower. On the other hand, it is not entirely fair to compare KDE-based methods directly, as they do not require a training process. Theoretically, estimating a distribution accurately with a small number of samples is nearly impossible. Therefore, it is also necessary to evaluate whether the trained neural networks can outperform the baseline methods when a sufficient number of samples are provided. Table IV V VI present the MSE and range comparisons between the proposed method (can have only 100 visible samples) and two baseline methods, given 2000 visible samples on three test distributions. While the results of the two baseline methods show slight improvements, they still fall significantly short of the performance achieved by our method.

Second, we want to ensure the convex bound generated by the neural networks is correct and useful. Table VII shows the performance of the neural network on 2d-binomial distribution. The neural network gets at least 98.7% correctness rate and only misses a few tests. Meanwhile, the average area we got is not significantly larger than the optimal area especially when α is 80%. As α increases, the difference between our area and the optimal area also increases. To guarantee reaching the confidence level, the neural networks tend to cover slightly more of the distribution. Since the distribution samples become sparser in the area far from the

2d-binomial	NN(our method)	BB(2000)	ILP(2000)
confidence level	MSE(range)	MSE(range)	MSE(range)
80%	0.42%(79.12% - 82.05%)	16.26%(93.24% - 98.43%)	4.12%(72.01% - 86.43%)
85%	0.35%(84.45% - 86.63%)	12.10%(95.65% - 98.49%)	3.15%(74.27% - 93.60%)
90%	0.24%(89.51% - 91.01%)	8.12%(96.52% - 99.63%)	4.37%(89.70% - 98.32%)
95%	0.62%(94.08% - 96.29%)	4.28%(98.64% - 99.86%)	3.22%(95.48% - 99.53%)
99%	0.87%(97.66% - 99.94%)	0.93%(99.73% - 99.99%)	0.86%(99.49% - 99.98%)

TABLE IV: MSE and range on 2d-binomial distribution distribution compare to baseline with a large number of sample

fanshape	NN(our method)	BB(2000)	ILP(2000)
confidence level	MSE(range)	MSE(range)	MSE(range)
80%	0.32%(78.95% - 80.44%)	12.73%(88.66% - 96.29%)	2.01%(75.36% - 84.46%)
85%	0.25%(84.44% - 86.21%)	10.98%(91.93% - 98.82%)	2.31%(81.43% - 90.18%)
90%	0.23%(89.40% - 90.91%)	8.63%(95.93% - 99.75%)	1.90%(87.40% - 94.16%)
95%	0.49%(95.22% - 96.02%)	4.81%(98.59% - 100%)	2.72%(94.35% - 99.06%)
99%	0.98%(99.96% - 99.99%)	0.99%(99.96% - 100%)	0.98%(99.19% - 100%)

TABLE V: MSE and range on fanshape distribution distribution compare to baseline with a large number of sample

GMR trajectory predictor	NN(our method)	BB(6000)	ILP(6000)
confidence level	MSE(range)	MSE(range)	MSE(range)
80%	1.79%(79.54% - 84.27%)	10.47%(85.60% - 93.33%)	2.40%(75.00% - 81.90%)
85%	1.76%(82.34% - 88.25%)	9.45%(90.69% - 96.35%)	3.01%(85.60% - 93.33%)
90%	1.13%(88.31% - 91.8%)	7.44%(95.89% - 98.67%)	1.37%(85.62% - 94.55%)
95%	0.85%(94.14% - 97.83%)	4.22%(97.98% - 99.67%)	0.74%(92.35% - 97.50%)
99%	0.58%(99.18% - 99.94%)	0.91%(99.72% - 99.97%)	0.25%(98.28% - 99.61%)

TABLE VI: MSE and range on GMR trajectory predictor distribution compare to baseline with a large number of sample

2d-binomial	correctness rate					
confidence level	NN	BB(100)	BB(2000)	ILP(100)	ILP(2000)	optimal(10000)
80%	99.7%	100%	100%	31.4%	14.7%	100%
85%	99.8%	100%	100%	67.3%	57.9%	100%
90%	99.8%	100%	100%	97.2%	99.8%	100%
95%	98.9%	99.9%	100%	99.1%	100%	100%
99%	98.7%	95.2	100%	99.9%	100%	100%
confidence level	PRS area					
80%	35.22	45.65	46.14	36.06	33.95	33.01
85%	41.58	52.16	50.12	42.42	40.69	34.23
90%	51.38	63.18	59.10	53.86	52.35	42.79
95%	64.53	75.85	71.90	67.46	66.08	55.01
99%	99.03	101.49	106.67	95.28	96.10	73.96

TABLE VII: correctness rate/PRS area for each desired confidence level on 2d-binomial distribution

fanshape	correctness rate					
confidence level	NN	BB(100)	BB(2000)	ILP(100)	ILP(2000)	optimal(10000)
80%	98.7%	100%	100%	57.7%	79.8%	100%
85%	99.8%	100%	100%	52.4%	64.4%	100%
90%	99.7%	99.8%	100%	52.8%	82.3%	100%
95%	100%	99.4%	100%	74.8%	98.9%	100%
99%	100%	61%	100%	59.7%	100%	100%
confidence level	PRS area					
80%	1415.07	2342.52	2309.52	1783.52	1514.04	1172.71
85%	1762.30	2790.63	2815.55	2138.71	1902.27	1579.52
90%	2229.01	3367.96	3470.37	2652.60	2365.27	2107.79
95%	3530.87	4525.46	4576.97	3382.33	3374.61	2742.49
99%	4833.31	5749.98	6127.58	4967.29	4820.67	3711.22

TABLE VIII: correctness rate/PRS area for each desired confidence level on fanshape distribution

GMR trajectory predictor	correctness rate					
confidence level	NN	BB(300)	BB(6000)	ILP(300)	ILP(6000)	optimal(30000)
80%	93.1%	100%	100%	10.8%	3.9%	100%
85%	95.2%	100%	100%	27.9%	16.2%	100%
90%	99.8%	100%	100%	69.2%	55.8%	100%
95%	95.6%	100%	100%	68.2%	65.4%	100%
99%	100%	99.7%	100%	56.5%	75.8%	100%
confidence level	PRS area					
80%	2.75E-3	3.64E-3	3.46E-3	2.59E-3	2.39E-3	2.15E-3
85%	3.44E-3	4.41E-3	4.35E-3	2.99E-3	2.89E-3	2.39E-3
90%	4.41E-3	7.37E-3	5.81E-3	3.83E-3	3.67E-3	2.99E-3
95%	5.69E-3	7.89E-3	7.98E-3	5.03E-3	4.87E-3	3.95E-3
99%	9.21E-3	11.19E-3	11.16E-3	8.01E-3	7.63E-3	6.46E-3

TABLE IX: correctness rate/PRS area for each desired confidence level on GMR trajectory predictor distribution

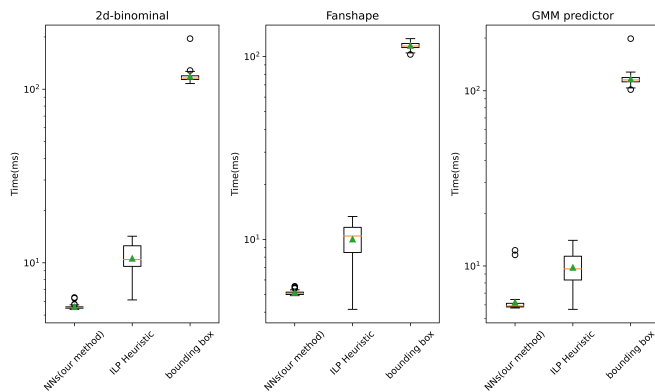


Fig. 8: Generating speed comparison

mean, even a small increase in coverage results in a significant increase in the area. Compared to the bounding box, while it may achieve a higher correctness rate due to its highly conservative nature, its area is significantly larger than that of the proposed method. Meanwhile, although the area of ILP is similar to that of NN, its correctness rate is significantly lower. Table VIII shows the performance of the neural network on fanshape distribution. The neural network achieves a near-perfect correctness rate of close to 100%. Additionally, the area comparison follows a similar trend to that observed in the 2d binomial distribution. Table IX shows the performance of the neural network on GMR trajectory predictor distribution. Although the correctness rate is not as high as in the previous tables, it still reaches a minimum of 93.1%. Meanwhile, the area remains superior to the Bounding Box, comparable to ILP, and only slightly larger than the optimal solution.

In summary, the proposed neural network demonstrates consistently high correctness rates across various distributions, ranging from at least 93.1% to nearly 100%, while maintaining a compact area that is only marginally larger than the optimal solution. This balance between correctness and efficiency underscores the utility of the neural network-generated convex sets. The result supports that the *Advantage 1* of the proposed method, NN can generate useful PRS with only a few samples.

C. Generating speed

In addition to comparing the accuracy, we compare the generating time required to generate useful results. Fig. 8 illustrates the average time cost for generating effective outcomes. The results clearly demonstrate that our method significantly outperforms the baseline approaches, achieving execution times that are an order of magnitude faster. The result supports that the *Advantage 2* of the proposed method, NN can generate useful PRS very fast.

VI. CONCLUSION AND FUTURE

In this paper, we propose using self-supervised learning to train a transformer-based neural network to generate convex approximations of probabilistic reachable sets. Once trained, the neural network can robustly generate convex approximations that cover the desired percentage of points sampled from

the distribution of the probabilistic reachable set only given a few samples from the distribution. The primary advantage of the proposed method is its extremely fast generation time while maintaining performance comparable to that of the baseline methods. Meanwhile, training is also very simple because training inputs can be generated very fast. Only a few experts are required for the labels. No physical information about the system such as disturbance is required.

ACKNOWLEDGMENT

The authors would like to acknowledge the support from the National Science Foundation under Grants CCF-2402689 and CMMI-2138612. Any opinions, findings, conclusions, or recommendations expressed in this paper are those of the authors and do not reflect the views of NSF.

REFERENCES

- [1] E. L. Thompson, A. G. Taye, W. Guo, P. Wei, M. Quinones, I. Ahmed, G. Biswas, J. Quattrociochi, S. Carr, U. Topcu *et al.*, “A survey of evtol aircraft and aam operation hazards,” in *AIAA AVIATION 2022 Forum*, 2022, p. 3539.
- [2] Y. Zhou and J. S. Baras, “Reachable set approach to collision avoidance for uavs,” in *2015 54th IEEE Conference on Decision and Control (CDC)*. IEEE, 2015, pp. 5947–5952.
- [3] Y. Lin and S. Saripalli, “Collision avoidance for uavs using reachable sets,” in *2015 International Conference on Unmanned Aircraft Systems (ICUAS)*. IEEE, 2015, pp. 226–235.
- [4] H. El-Kebir and M. Ornik, “Online inner approximation of reachable sets of nonlinear systems with diminished control authority,” in *2021 Proceedings of the Conference on Control and its Applications*. SIAM, 2021, pp. 9–16.
- [5] X. Yang, B. Mu, D. Robertson, and J. Scott, “Guaranteed safe path and trajectory tracking via reachability analysis using differential inequalities,” *Journal of Intelligent & Robotic Systems*, vol. 108, no. 4, p. 78, 2023.
- [6] M. Althoff, G. Frehse, and A. Girard, “Set propagation techniques for reachability analysis,” *Annual Review of Control, Robotics, and Autonomous Systems*, vol. 4, no. 1, pp. 369–395, 2021.
- [7] X. Chen and S. Sankaranarayanan, “Reachability analysis for cyber-physical systems: Are we there yet?” in *NASA formal methods symposium*. Springer, 2022, pp. 109–130.
- [8] S. Jafarpour, Z. Liu, and Y. Chen, “Probabilistic reachability analysis of stochastic control systems.”
- [9] T. Lew, A. Sharma, J. Harrison, A. Bylard, and M. Pavone, “Safe active dynamics learning and control: A sequential exploration–exploitation framework,” *IEEE Transactions on Robotics*, vol. 38, no. 5, pp. 2888–2907, 2022.
- [10] M. Chen, S. L. Herbert, M. S. Vashishtha, S. Bansal, and C. J. Tomlin, “Decomposition of reachable sets and tubes for a class of nonlinear systems,” *IEEE Transactions on Automatic Control*, vol. 63, no. 11, pp. 3675–3688, 2018.
- [11] R. E. Allen, A. A. Clark, J. A. Starek, and M. Pavone, “A machine learning approach for real-time reachability analysis,” in *2014 IEEE/RSJ international conference on intelligent robots and systems*. IEEE, 2014, pp. 2202–2208.
- [12] M. E. Cao, M. Bloch, and S. Coogan, “Estimating high probability reachable sets using gaussian processes,” in *2021 60th IEEE Conference on Decision and Control (CDC)*. IEEE, 2021, pp. 3881–3886.
- [13] A. Devonport and M. Arca, “Data-driven reachable set computation using adaptive gaussian process classification and monte carlo methods,” in *2020 American control conference (ACC)*. IEEE, 2020, pp. 2629–2634.
- [14] M. Fiacchini and T. Alamo, “Probabilistic reachable and invariant sets for linear systems with correlated disturbance,” *Automatica*, vol. 132, p. 109808, 2021.
- [15] A. Dosovitskiy, L. Beyer, A. Kolesnikov, D. Weissenborn, X. Zhai, T. Unterthiner, M. Dehghani, M. Minderer, G. Heigold, S. Gelly *et al.*, “An image is worth 16x16 words: Transformers for image recognition at scale,” *arXiv preprint arXiv:2010.11929*, 2020.

- [16] A. Vaswani, N. Shazeer, N. Parmar, J. Uszkoreit, L. Jones, A. N. Gomez, Ł. Kaiser, and I. Polosukhin, "Attention is all you need," *Advances in neural information processing systems*, vol. 30, 2017.
- [17] D. Liu, M. Jiang, and K. Pister, "Llmeasyquant—an easy to use toolkit for llm quantization," *arXiv preprint arXiv:2406.19657*, 2024.
- [18] Y. Weng and J. Wu, "Leveraging artificial intelligence to enhance data security and combat cyber attacks," *Journal of Artificial Intelligence General science (JAIGS) ISSN: 3006-4023*, vol. 5, no. 1, pp. 392–399, 2024.
- [19] H. Mojtahed, R. Rao, C. Paolini, and M. Sarkar, "Temporal modeling of instantaneous interbeat interval based on physical activity," *IEEE Access*, 2023.
- [20] Z. Wang, Y. Zhu, M. Chen, M. Liu, and W. Qin, "Llm connection graphs for global feature extraction in point cloud analysis," *Applied Science and Biotechnology Journal for Advanced Research*, vol. 3, no. 4, pp. 10–16, 2024.
- [21] J. Wang, W. Chi, C. Li, C. Wang, and M. Q.-H. Meng, "Neural rrt*: Learning-based optimal path planning," *IEEE Transactions on Automation Science and Engineering*, vol. 17, no. 4, pp. 1748–1758, 2020.
- [22] J. Wang, X. Jia, T. Zhang, N. Ma, and M. Q.-H. Meng, "Deep neural network enhanced sampling-based path planning in 3d space," *IEEE Transactions on Automation Science and Engineering*, vol. 19, no. 4, pp. 3434–3443, 2021.
- [23] S. Liu and M. Zhu, "Learning multi-agent behaviors from distributed and streaming demonstrations," *Advances in Neural Information Processing Systems*, vol. 36, 2024.
- [24] —, "Distributed inverse constrained reinforcement learning for multi-agent systems," *Advances in Neural Information Processing Systems*, vol. 35, pp. 33 444–33 456, 2022.
- [25] K. Li, J. Chen, D. Yu, T. Dajun, X. Qiu, L. Jieting, S. Baiwei, Z. Shengyuan, Z. Wan, R. Ji *et al.*, "Deep reinforcement learning-based obstacle avoidance for robot movement in warehouse environments," *arXiv preprint arXiv:2409.14972*, 2024.
- [26] K. Mo, L. Chu, X. Zhang, X. Su, Y. Qian, Y. Ou, and W. Pretorius, "Dral: Deep reinforcement adaptive learning for multi-uavs navigation in unknown indoor environment," *arXiv preprint arXiv:2409.03930*, 2024.
- [27] K. Li, J. Wang, X. Wu, X. Peng, R. Chang, X. Deng, Y. Kang, Y. Yang, F. Ni, and B. Hong, "Optimizing automated picking systems in warehouse robots using machine learning," *arXiv preprint arXiv:2408.16633*, 2024.
- [28] K. Hornik, M. Stinchcombe, and H. White, "Multilayer feedforward networks are universal approximators," *Neural networks*, vol. 2, no. 5, pp. 359–366, 1989.
- [29] J. Zhang, Y. Cheng, and X. He, "Fault diagnosis of energy networks based on improved spatial-temporal graph neural network with massive missing data," *IEEE Transactions on Automation Science and Engineering*, 2023.
- [30] J. Li, Y. Chen, and Y. Xing, "Memory mechanism for unsupervised anomaly detection," in *The 39th Conference on Uncertainty in Artificial Intelligence*, 2023.
- [31] H.-C. Dan, B. Lu, and M. Li, "Evaluation of asphalt pavement texture using multiview stereo reconstruction based on deep learning," *Construction and Building Materials*, vol. 412, p. 134837, 2024. [Online]. Available: <https://www.sciencedirect.com/science/article/pii/S0950061823045580>
- [32] V. Hegde and S. Usmani, "Parallel and distributed deep learning," *May*, vol. 31, pp. 1–8, 2016.
- [33] K. He, X. Chen, S. Xie, Y. Li, P. Dollár, and R. Girshick, "Masked autoencoders are scalable vision learners," in *Proceedings of the IEEE/CVF conference on computer vision and pattern recognition*, 2022, pp. 16 000–16 009.
- [34] H. Ni, S. Meng, X. Geng, P. Li, Z. Li, X. Chen, X. Wang, and S. Zhang, "Time series modeling for heart rate prediction: From arima to transformers," *arXiv preprint arXiv:2406.12199*, 2024.
- [35] P. Sun, H. Kretzschmar, X. Dotiwalla, A. Chouard, V. Patnaik, P. Tsui, J. Guo, Y. Zhou, Y. Chai, B. Caine *et al.*, "Scalability in perception for autonomous driving: Waymo open dataset," in *Proceedings of the IEEE/CVF conference on computer vision and pattern recognition*, 2020, pp. 2446–2454.
- [36] I. Navarro, P. Ortega, J. Patrikar, H. Wang, Z. Ye, J. H. Park, J. Oh, and S. Scherer, *AmeliaTF: A Large Model and Dataset for Airport Surface Movement Forecasting*. [Online]. Available: <https://arc.aiaa.org/doi/abs/10.2514/6.2024-4251>
- [37] M. Gilles, Y. Chen, E. Z. Zeng, Y. Wu, K. Furmans, A. Wong, and R. Rayyes, "Metagraspnetv2: All-in-one dataset enabling fast and reliable robotic bin picking via object relationship reasoning and dexterous grasping," *IEEE Transactions on Automation Science and Engineering*, 2023.
- [38] P. Wu, S. Martinez, and J. Chen, "Fine-tuned convex approximations of probabilistic reachable sets under data-driven uncertainties," *IEEE Transactions on Automation Science and Engineering*, 2024.
- [39] P. Wu and J. Chen, "Data-driven polytopic approximation for an n -dimensional probabilistic reachable set," *IEEE Transactions on Industrial Informatics*, 2024.
- [40] —, "Efficient box approximation for data-driven probabilistic geofencing," *Unmanned Systems*, pp. 1–12, 2023.
- [41] S. T. Barratt, M. J. Kochenderfer, and S. P. Boyd, "Learning probabilistic trajectory models of aircraft in terminal airspace from position data," *IEEE Transactions on Intelligent Transportation Systems*, vol. 20, no. 9, pp. 3536–3545, 2018.
- [42] J. Xiang and J. Chen, "Data-driven probabilistic trajectory learning with high temporal resolution in terminal airspace," *arXiv preprint arXiv:2409.17359*, 2024.
- [43] —, "Imitation learning-based convex approximations of probabilistic reachable sets," in *AIAA AVIATION FORUM AND ASCEND 2024*, 2024, p. 4356.
- [44] T. Hastie, R. Tibshirani, J. H. Friedman, and J. H. Friedman, *The elements of statistical learning: data mining, inference, and prediction*. Springer, 2009, vol. 2.
- [45] W. Zhao and R. Wen, "The algorithm of fast collision detection based on hybrid bounding box," in *2012 International Conference on Computer Science and Electronics Engineering*, vol. 3. IEEE, 2012, pp. 547–551.
- [46] C. Ericson, *Real-time collision detection*. Crc Press, 2004.
- [47] P. Wu and J. Chen, "Data-driven zonotopic approximation for n -dimensional probabilistic geofencing," *Reliability Engineering & System Safety*, vol. 244, p. 109923, 2024.



Jun Xiang is currently pursuing the joint Ph.D. degree at the Department of Mechanical and Aerospace Engineering, University of California at San Diego, and the Department of Aerospace Engineering, San Diego State University. He received his M.S. degree in Automotive Engineering from Clemson University and his B.S. degree in Mechanical Engineering from North Carolina State University. His research interests include motion planning and prediction of autonomous air/ground vehicle systems.



Jun Chen is an Associate Professor of Aerospace Engineering at San Diego State University. He received his M.S. and Ph.D. degrees in Aerospace Engineering from Purdue University. His research interests include control and optimization for large-scale networked dynamical systems, with applications in mechanical and aerospace engineering such as air traffic control, traffic flow management, and autonomous air/ground vehicle systems.